

Competition between Magnetic and Structural Transitions in CrN

A. Filippetti, W. E. Pickett and B. M. Klein

Department of Physics, University of California – Davis, Davis, Ca 95616

CrN is observed to undergo a paramagnetic to antiferromagnetic transition with Néel temperature $T_N \sim 280$ K, accompanied by a shear distortion from cubic NaCl-type to orthorhombic Pnma structure. Our first-principles plane wave calculations, based on ultrasoft pseudopotentials, confirm that the distorted antiferromagnetic phase with spin configuration arranged in double ferromagnetic sheets along the [110] direction is energetically much more stable than the paramagnetic phase, and also slightly favored over the ferromagnetic and other examined antiferromagnetic phases. The energy gain from polarization is much larger than that from distortion; nevertheless, the distortion is decisive in resolving the competition among the antiferromagnetic phases: the anisotropy in the (100) plane arising from the ferromagnetic double-sheet magnetic order allows a small but important energy gain upon the cubic-to-orthorhombic transition. Although antiferromagnetic order leads to a large depletion of states around Fermi level, it does not open a gap. The system is metallic with occupied hole and electron pockets of Fermi surface containing ~ 0.025 carriers of each sign per formula unit. The simultaneous occurrence of structural distortion and antiferromagnetic order, as well as the competition between antiferromagnetism and ferromagnetism, is analyzed.

71., 75., 71.15.Hx, 75.50.Ee

I. INTRODUCTION

3d transition metal mono-nitrides (TMN) are interesting technologically due to a rich variety of properties, ranging from high- T_c superconductivity (observed in TiN and VN), to very hard surface coatings, to heterogeneous catalysis¹. Although some characteristics are common to the whole series of compounds such as having high melting points and chemical hardnesses, this class also exhibits interesting variation in some properties. ScN is semiconducting², as CrN is sometimes reported³ to be, while TiN and VN are superconductors⁴. Regarding magnetic properties, ScN, TiN and VN are paramagnets³, CoN has been only recently synthesized⁵ and is also found paramagnetic. For CrN, strong experimental evidence supports antiferromagnetism below a Néel temperature $T \sim 273$ - 286 K^{3,6-9}, and recent measurements suggest for FeN antiferromagnetism¹⁰ as well.

Even for the structural properties there is no uniformity. Most of compounds have rocksalt structure, but there are exceptions: CoN has ZnS-type structure⁵, and FeN has been observed in both ZnS- and NaCl-type phases (depending on the growth conditions). CrN seems

to be very peculiar in that it is the only one of the series that does not have a ground state with cubic symmetry. Its transition from paramagnetism to antiferromagnetism at T_N is accompanied by a structural distortion from cubic to orthorhombic (Pnma) symmetry⁶.

The body of information on 3d TMN properties is rather fragmentary (and sometime contradictory), and much vital data are unavailable. Most of these compounds are difficult to synthesize, and the strong tendency of nitrogen to form dimers leads to difficulty in growing defect-free TMN crystals³ (a problem also common to other nitride compounds such as III-V semiconductors). Thus far, nothing is known about MnN, NiN, CuN and ZnN, and only recently it has become possible to synthesize FeN¹⁰ and CoN⁵.

Due to the difficulty in preparing stoichiometric CrN, and to a strong sensitivity of its properties on the concentration of defects, reports on the properties of CrN in the literature are not entirely consistent. Browne *et al.*⁸ have studied the effects of variation of x in CrN_x and produced samples with x up to 0.997, taking care to keep them oxygen-free. Only at this high N composition is the antiferromagnetic transition sharp, and it occurs at $T_N=286$ K. The transformation is first order, with hysteresis of 2-3 K as measured by linear expansivity, susceptibility, and resistivity. At lower values of x (down to 0.980) the transition temperature decreases to 273 K and the transition width increases.

At $x=0.997$, the properties reported by Browne *et al.* are as follows. The resistivity slope $d\rho/dT$ is positive (metallic-like) on both sides of the transition, and ρ decreases by 30-35% across the transition, in opposition to the semiconducting behavior reported by Herle *et al.*³ Due to the polycrystalline nature, and specific density only 70% of the bulk, the value of the resistivity $\sim 2 - 3m\Omega cm$ is only an upper bound. The susceptibility slope changes from a small negative value $d\log\chi/dT \sim -4 \times 10^{-4} \text{ K}^{-1}$ above T_N to a positive value of similar magnitude below T_N . The decrease in χ is $\sim 35\%$. These data are most consistent with a metal-to-metal transition at T_N in which a substantial fraction of the Fermi surface is gapped by structural distortion and/or the onset of magnetic order. Tsuchiya *et al.*¹¹ have produced thin films of CrN_x with $1.0 \leq x \leq 1.2$. These films, like the samples with $x \leq 1$ of Browne *et al.*, have $T_N \leq 280$ K. None of the transitions are as sharp as for the $x = 0.997$ samples. It is clear that properties are sensitive to N overstoichiometry as well as to understoichiometry.

Not surprisingly, the theoretical literature is also not very extensive. Some work on the 3d TMNs in the cu-

bic paramagnetic phase has been reported^{12–15}, but very little is reported for compounds that undergo reconstructions accompanied by, and perhaps driven by, magnetic ordering, as may be the case in CrN¹⁷ and FeN¹⁶. Investigation of compounds that are so close in chemical composition but with so different physical properties are important in providing insight into basic mechanisms such as magnetic ordering, formation of local moments, and relations of this phenomena with basic features such as structure and density of states. Ab initio calculations, which can separate the effects of magnetism and structural distortions, are very effective in such cases. In this paper we focus on CrN and investigate the occurrence of magnetic ordering for the cubic structure and for the (observed) orthorhombic structure.

A basic characteristic of CrN in the cubic paramagnetic phase, which makes it easy to understand the instability towards ferromagnetism, is the very high density of states¹² at the Fermi energy (E_F). Less easy to understand is the competition between AFM and FM ordering, and the relation between spin polarization, magnetic order, and structural distortion. Other cases are well known where high DOS drives systems to structural (e.g. VO₂, from tetragonal to monoclinic) or spin polarized (CrO₂, from PM to half-metallic FM) transitions. In fact, the isovalent compound MoN shows an interesting parallel. Due to the peak at E_F in the density of states in the cubic phase, it was predicted to be a high temperature superconductor¹⁹ (compared to conventional superconductors). It was subsequently shown by calculation²⁰ that it is structurally unstable in the cubic structure, which explains the fact that experimentalists had been unable to grow stoichiometric samples. In the case of CrN the cubic structure is stable at high temperature, but at T_N there is the simultaneous occurrence of both structural transformation and magnetic order. Giving insight into possible relations between these transitions, and identifying the driving force for the transition, is the main motivation of the present work.

The paper is organized as follows: in Section II a review of the CrN crystal structure is given, together with a brief description of our calculational procedure. In Section III we show structural and energetic results for CrN in different magnetic phases. Finally, Section IV is dedicated to an analysis of the electronic properties. Results for density of states, band energies, and some Fermi surface properties are presented and discussed.

II. CRYSTAL STRUCTURE AND METHOD OF CALCULATION

In Figure 1 a tridimensional perspective (top panel) and a top view down onto the (001) plane (bottom panel) of the CrN structure is shown. The \hat{x} , \hat{y} and \hat{z} axes of the unit cell for the AFM phase are oriented along the $[1\bar{1}0]$, $[110]$ and $[001]$ directions of the cubic NaCl

structure, respectively. The shear distortion consists of a contraction (not visible in the Figure) of the angle α from the cubic ($\alpha=90^\circ$) to a $\sim 2^\circ$ smaller observed value. The square symmetry in the (001) plane is broken so that the coordination of the atoms reduces to 2 in the (001) plane. Orthorhombic and cubic structures are connected by the relations $a = 2a_0\sin(\alpha/2)$, $b = a_0\cos(\alpha/2)$ and $c = a_0$.

From experiments, two possible antiferromagnetic spin alignments have been proposed^{6,9}. We consider here primarily the arrangement determined by Corliss *et al.*⁶ and depicted by arrows on Cr sites in Figure 1: double ferromagnetic layers parallel to the $[110]$ direction alternate in such a way to form a four-layer antiferromagnetic orthorhombic unit cell (4 formula units and 8 atoms per cell), with non vanishing magnetization field planarly averaged along $[1\bar{1}0]$. As a result of this ordering, six of the 12 (cubic) Cr neighbors have spin parallel and six spin antiparallel. Of the six (cubic) next nearest neighbors, four have antiparallel spin. Ref. 6 reports for the magnetic moments $m = 2.36 \mu_B$ per Cr atom. Another experiment⁷ gives a much larger $m = 3.17 \mu_B$ that seems to be much less reasonable. Indeed, the first value is consistent with a Cr to N charge transfer of $\simeq 2$ electrons, while the second would imply an almost completely ionized configuration $\text{Cr}^{+(3-\delta)}\text{N}^{-(3-\delta)}$ that is not to be expected (charge transfer would be larger than in more ionic compounds such as transition-metal oxides).

Another motivation for this work is technical and centers on our method of calculation. These local-spin-density calculations are performed within a plane wave and ultrasoft pseudopotential²² (USPP) framework. Here we want to furnish a sound assessment of accuracy and efficiency of the use of pseudopotentials for the study of materials historically considered impossible, or at best difficult, to be treated within a plane wave pseudopotential method. CrN is a difficult test, being the combination of a $3d$ transition metal and a first-row atom, with high density of states at E_F and a reconstruction accompanied by antiferromagnetism.

To our knowledge this is the first plane-wave study of AFM CrN (only one augmented-spherical-wave calculation¹⁷ is present in literature). Use of USPP for magnetic materials is very new^{23,25} and presents the essential feature: constructing smooth (but well transferable) USPP allows us to obtain converged results at energy cut-off of 29 Ry (~ 2600 plane waves per CrN unit), whereas ordinary norm-conserving pseudopotentials would require at least the twice as large a cutoff value, hence four times as many plane waves. The non-linear core correction²⁴, particularly important for spin-polarized situations²³, was used to ensure the best degree of transferability. The exchange-correlation potential was that of Ceperley and Alder, as parametrized by Perdew and Zunger²¹. We sampled the irreducible zone (IBZ) with well converged series of special k-points (~ 30 for self-consistent calculations, from 150 up to 530 k points to evaluate the densities of states).

III. STRUCTURAL PROPERTIES

In Table I our results for energies and magnetic moments of PM, FM and AFM phases of CrN are shown. For a fair comparison between theory and experiment we investigated, together with the AFM double-sheet ordering found by Corliss *et al* (here indicated as $\text{AFM}_{[110]}^2$), other two kinds of AFM orderings: the single-sheet $\text{AFM}_{[110]}^1$ phase, similar to the $\text{AFM}_{[110]}^2$ but with single ferromagnetic sheets having alternated spin along [110] (a tetragonal structure with 4 atoms per cell), and the $\text{AFM}_{[111]}$ phase, consisting on single ferromagnetic sheets parallel to the (111) plane which alternate the sign of the spin along [111] (i.e. a trigonal structure common in 3d transition metal monoxides with 6 Cr and 6 N layers in the cell). For each phase, we present results obtained in both cubic and distorted structures. For the cubic structures we consider both experimental and theoretical lattice constants (i.e. the a_0 obtained by energy minimization of the respective phases). To add the further effect of the planar distortion, we extract the value of α from the experimental structure given in Ref. 6 ($\alpha=88.23^\circ$).

A number of results for the PM cubic (NaCl) phase of CrN are present in literature^{17,12,16}. In particular, Shimizu, Shirai, and Suzuki¹⁶ performed lattice constant calculations for the whole series of 3d TMN's. For CrN they report $a_0^{PM}=7.56$ a.u. which underestimates the experimental value $a_0^{exp}=7.81$ a.u. for the $\text{AFM}_{[110]}^2$ phase (a 10% smaller volume). Our calculation gives $a_0^{PM}=7.73$ a.u., a value 1% smaller than experiment. For a true comparison, however, it is necessary to calculate the lattice constant for the cubic $\text{AFM}_{[110]}^2$ structure. We find $a_0^{AFM}=7.876$ a.u., less than 1% above experiment. Thus, according to our calculations, polarization (from PM to $\text{AFM}_{[110]}^2$ order) produces an expansion of 2% of the lattice constant.

Looking at Table I, we see that the $\text{AFM}_{[110]}^2$ distorted phase is favoured overall. The theoretical determination of a_0 produces, with respect to the experimental structure, an energy gain ($E_d^{ex}-E_d^{th}$) of 0.02 eV/formula unit; anyway, in general, results obtained for theoretical and experimental lattice constants are close each other to within 0.01 eV. The spin polarization PM to AFM gives a considerable energy gain (~ 0.15 eV to ~ 0.3 eV per formula unit, depending on the magnetic phase), thus, polarization greatly lowers the energy regardless of the type of magnetic order. This is a sign that there is likely to be disordered local moment behavior above T_N , although it is not so evident from the existing data.⁸ Also, all AFM phases are more stable than the FM one.

Now, we examine in more detail the competition among the different AFM phases. The $\text{AFM}_{[111]}$ is worthwhile to be considered because it represents the usual kind of AFM order observed for NaCl-type structures. Indeed, a peculiarity of the $\text{AFM}_{[111]}$ phase (unless one considers noncollinear arrangements) is having all the

six (fcc) second neighbor moments antiparallel, a common characteristic of most of NaCl structures, as revealed by neutron diffraction studies¹⁸. Nevertheless, we found the $\text{AFM}_{[111]}$ clearly disfavoured with respect to the $\text{AFM}_{[110]}^2$ and only slightly favoured on the FM phase. More interesting and somewhat surprising is the result for the $\text{AFM}_{[110]}^1$ phase: we found it to be clearly the most stable of the cubic structures. It is characterized by four spin-parallel and eight spin-antiparallel first neighbors, and all the six second neighbors have parallel spins (an arrangement very different from the other AFM phases here considered). But if the planar distortion is added, the energetic order of $\text{AFM}_{[110]}^1$ and $\text{AFM}_{[110]}^2$ phases is reversed, and the $\text{AFM}_{[110]}^2$ becomes the lowest, thus recovering the agreement with the experiment. Indeed, the distortion causes, for the $\text{AFM}_{[110]}^2$, the shortening of metal-metal distances between spin-antiparallel Cr atoms, that arguably causes an energy gain, and the stretching of spin-parallel Cr atoms in the (100) plane (producing an energy loss), resulting, as a matter of fact, in an appreciable net decrease of energy (~ 0.07 eV/formula unit). The same cannot occur for the $\text{AFM}_{[110]}^1$, because no spin-antiparallel first neighbors are in the (100) plane, and thus the distortion does not allow any stabilization (actually we found an energy increase of ~ 0.01 eV/formula unit).

Thus, the resulting physical picture is the following: if we consider the spin ordering in a constrained cubic symmetry, the $\text{AFM}_{[110]}^1$ phase, having the largest number of fcc spin-antiparallel first-neighbors (8, against 6 of both $\text{AFM}_{[110]}^2$ and $\text{AFM}_{[111]}$ phases) is favoured. But if we allow the symmetry to relax, the (100) planar anisotropy of the $\text{AFM}_{[110]}^2$ phase causes some of the spin-antiparallel first neighbors to approach each other, producing a strong structural stabilization. We argue that in the cubic structure the bonds between spin-antiparallel metal atoms are under condition of large tensile stress (larger than that in the bonds between spin-parallel atoms, anyway) and the cubic to orthorhombic transition relieves part of this stress. Then, the planar distortion plays a key role in the competition between AFM phases, and the stress relief is reasonably to be considered the ultimate driving force towards distortion.

For magnetic moments (we show in the Table only values referred to the experimental structures, being very close to that obtained for the theoretical ones) we obtain values ranging between $m=1.9 \mu_B$ and $2.3 \mu_B$ per Cr atom. In particular, for the $\text{AFM}_{[110]}^2$ phase our value $m=2.15 \mu_B$ is in fair agreement with the experimental $m=2.36 \mu_B$ of Ref. 6, and the theoretical $m=2.41 \mu_B$ of Ref. 17.

IV. ELECTRONIC PROPERTIES

A. Effect of AFM_[110]² Ordering

The stabilization due to the magnetic ordering can be understood from the analysis of the density of states (DOS). Figure 2 shows the PM CrN DOS for the cubic structure in orthorhombic symmetry obtained from broadened eigenvalues from a regular mesh of k points in the irreducible zone, which is sufficient for our purposes. Unless otherwise indicated, in what follows all quantities refer to the theoretical lattice constant. As pointed out previously¹², among the series of 3d TMNs, CrN (as well as NaCl-type FeN¹⁶) is distinguished for the high DOS at E_F . Our DOS agrees well with the full-potential linearized augmented plane wave calculation of Ref. 12. At least 95% of DOS at E_F comes from Cr d states, and the remaining contribution is due to the N p states. However, the DOS peak at E_F is *entirely* due to Cr d states, indicating that the peak arises from flat bands solely Cr in character. Singh and Klein²⁶ have emphasized that this peak is Cr t_{2g} . As we show below, it is not possible to identify this flat band solely from symmetry line data.

Figure 3 shows total and partial DOSs of the cubic AFM_[110]² structure. The peak at E_F has disappeared: the AFM_[110]² ordering causes a large band splitting and the depletion (a pseudogap ~ 0.5 eV wide) in the DOS of a sharp region around E_F .

Up- and down-polarized atoms are connected by translation plus spin-flip symmetry operations, thus contributions to DOS coming from the type of Cr and N atoms not shown in the Figure are equal to that shown but with up and down components interchanged. For N (middle panel of Figure 3) magnetic effects are negligible, although not zero by symmetry: the magnetic moments are only $\sim 0.01 \mu_B$. For Cr (bottom) the DOS around E_F clearly resembles the total one, hence the band splitting due to the polarization arises almost entirely from Cr d states.

B. Fermi Surface Properties

Notwithstanding the strong stabilization by moving states away from E_F , AFM_[110]² ordering does not manage to open a gap at the E_F , and the system is still a (relatively low carrier density) metal, at variance with one³ experimental characterization as a small gap semiconductor but in agreement with the results of Browne *et al.*⁸ on very nearly stoichiometric samples. To provide a clearer picture of our prediction, in Figure 4 we show a band-resolved DOS including only the four bands (see Section IV D) that cross or touch the Fermi level. These DOSs were calculated from a 528 k -points mesh, interpolated using a Fourier spline technique²⁷, and evaluated using the linear tetrahedron method. Full lines refer to the distorted (experimental) structure AFM_[110]² bands, while dashed lines refer to the cubic AFM_[110]² phase. Basically three bands contribute to the DOS at E_F , and a

fourth band has its minimum essentially at E_F .

In Table II the band-by-band values of the band filling, density of states at E_F , and the Fermi velocities are given. From the totals we can evaluate the Drude plasma energies $\hbar\Omega_p$:

$$\Omega_{p,j}^2 = 4\pi e^2 N(E_F) v_{F,j}^2, \quad (1)$$

where j denotes any of the Cartesian axes. We obtain $\hbar\Omega_{p,x} = 2.3$ eV, $\hbar\Omega_{p,y} = 2.0$ eV, $\hbar\Omega_{p,z} = 2.6$ eV, so the non-cubic nature is evident but is only a $\pm 15\%$ effect. This difference is due to the antiferromagnetism, not to the structural distortion whose effect we have found to be much smaller. These values of plasma energies are rather small for transition metal compounds, but are typical of metallic (not semiconducting or even semimetallic) behavior.

C. Analysis of Magnetic Structures

We mention a technical detail about calculation of magnetic moments. In case of an AFM structure with aligned spins along high symmetry directions, it is very suited for a plane-wave basis to extract magnetic moments from the planar average of local magnetization, which is a more direct and simple procedure than the common way of projecting plane waves onto atomic-like orbitals. In the top panel of Figure 5 the planar average of local magnetization along \hat{x} for the FM (dashed line) and AFM_[110]² (full line) phase is shown. Peaks are in correspondence of atomic positions, and the integrals over interlayer distances give by construction the layer-by-layer magnetization, i.e. the magnetization per couple chromium-nitrogen, or, in practice, the magnetization per Cr atom, being that of N atoms almost discardable. The idea to obtain contributions to some physical quantity coming from individual space regions, not accessible from its macroscopic (or 'integrated') value, using planar and macroscopic averages has been sometime used. It led, for example, to introduce quantities such as energy²⁸ and stress²⁹ density. In order to the integrals of the planar averages be well (uniquely) defined, a typical necessity is that the average is referred to an appropriate bulk symmetry plane (a critical case is, for instance, the average on (111) direction for a zincblende structure: the atomic layers are not equally spaced and the volume attained to a single atom is undefined). We return at Figure 5 below.

To complete the analysis of the DOS, in Figure 6 we present results for the FM phase of CrN in the experimental structure. As expected, the total DOS at the E_F is dominated by the Cr d states. Ferromagnetism results in the splitting of up and down d type bands, and a strong stabilization with respect to the PM phase occurs. The competition between antiferromagnetism and ferromagnetism for metals is usually an intriguing question. In the present case, we can attribute the stronger AFM

stability to a larger average spin splitting of Cr $3d$ states. It is clear from top panel of Figure 5 that for AFM $^2_{[110]}$ there is larger magnetization on the Cr atoms. This trend should also be reflected in the band splitting. A measure of the average band splitting per atom is taken to be:

$$\langle \Delta V_{xc} \rangle_m = \int_{S_j} dr \Delta V_{xc}(r) \cdot m(r) / \int_{S_j} dr m(r) \quad (2)$$

i.e. the up and down exchange-correlation potential difference ΔV_{xc} , weighted by the local magnetization, integrated over the inter-planar volume S_j and normalized to the atomic moment. The integrand of Equation 2 is pictured in the bottom panel of Figure 5; the supralinear dependence of Kohn-Sham potential on magnetization leads to the difference between AFM $^2_{[110]}$ (full line) and FM (dashed) $\Delta V_{xc}(\mathbf{r}) \cdot m(\mathbf{r})$ in the regions around the atoms, resulting in an integrated value (over the inter-planar distance) of 2.58 eV for the distorted AFM $^2_{[110]}$, 2.52 for the cubic AFM $^2_{[110]}$, and 2.02 eV for the distorted FM phase. The calculated splitting roughly reflects the magnitude visible in the Figures of DOS previously discussed. In Figure 7 an expanded view of the partial DOS of Cr around E_F is shown. Evidently, the AFM $^2_{[110]}$ DOS has a minimum at E_F , whereas for the FM system E_F falls on the edge of the second peak of Cr d states that is unoccupied in the PM phase (see Figure 2).

D. Band Shift from Magnetic Order and Lattice Distortion

The band splitting mechanism is further clarified by analysis of band shifts. Figures 8 and 9 show the PM and the AFM $^2_{[110]}$ band structures, respectively, calculated in the orthorhombic cell. The coordinates of the high-symmetry k-points are, in the orthorhombic reference system (see bottom panel of Figure 8), $M=(\pi/a,0,0)$, $X=(0,\pi/b,0)$, $L=(0,\pi/b,\pi/c)$, and $W=(\pi/a,3\pi/2b,0)$, where a , b , and c are given in Section II. In the cubic PM phase, at points M , X , W , and L all bands are doubly degenerate, due to the fcc to orthorhombic band downfolding. Symmetry breaking due to the AFM $^2_{[110]}$ ordering splits the degeneracy along the direction connecting points M and W , whereas the lattice shear ($\alpha \neq 90^\circ$) causes the band splitting at X and L . The former effect is the most effective in stabilizing the system. The splitting (~ 2 eV) strongly depletes the region around E_F , leaving only few band crossings. It is particularly visible at M by comparing cubic PM and AFM $^2_{[110]}$ band structures.

The effect of lattice shear produces a further stabilization, *i.e.* a further band opening, but is much less spectacular. It is emphasized in Figure 8: band energies shown along M - Γ - X are those of the cubic PM phase, whereas along X - W - L the Figure reports values for the distorted structure, so that the splitting is visible at X .

This effect is very small (its order of magnitude is only some tens of meV), and band structures of cubic and distorted AFM $^2_{[110]}$ phase (Figures 9 and 10) differ only in certain regions.

An unusual feature that can be seen in Figure 9 is the coincidence (or nearly so) of E_F with four band crossings along the directions shown: two along the M - Γ line, one along Γ - X , and one at W . At general k-points away from these crossings, the bands will repel, hence they will not contribute to $N(E_F)$, but rather to a pseudogap at E_F .

V. CONCLUSION

Our first principles results for CrN confirm most of the available experimental data. The observed (110) double-sheet distorted structure is found to be the lowest in energy, stable not only against paramagnetic and ferromagnetic phases, but also with respect to other antiferromagnetic arrangements. We found the system to be a weak metal, with large magnetic moments on Cr atoms.

Although the fundamental features favouring a certain spin arrangement with respect to another are still to be understood, we are able to clarify the role played by the distortion by disentangling its effect and that of the magnetic ordering. Magnetic ordering is found to be dominant in determining both structural and magnetic properties of the system, with respect to which the distortion can be seen as a small perturbation. Nevertheless, distortion appears decisive to resolve the competition among the different antiferromagnetic phases considered here. Indeed, it causes a meaningful energy gain for the (110) double-sheet phase, possibly due to relieving tensile stress stored in the spin-antiparallel metal-metal bonds.

Our calculations represent one of the first attempts to study magnetic systems within a framework of plane waves with ultrasoft pseudopotentials. All comparisons with previous available results confirm that the accuracy of this methodology is comparable to that of the all-electron calculations.

ACKNOWLEDGMENTS

This work was supported by National Science Foundation Grant No. DMR-9802076. Computations were carried out at the San Diego Supercomputing Center and at the Maui High Performance Computing Center.

¹ G. Linker, H. Schmidt, C. Politis R. Smithey and P. Ziemann, J. Phys. F Metal Phys. **161**, 2167 (1986); B. W. Roberts, J. Phys. Chem. Ref. Data **51**, 541 (1976).

² P. J. Dismukes, M. W. Yim and S. V. Ban, J. Crist. Growth **13/14**, 365 (1972).

³ P. Subramanya Herle, M. S. Hedge, N. Y. Vasathacharya and S. Philip, J. Solid. State Chem. **134**, 120 (1997).

⁴ H. F. George and H. K. John, Phys. Rev. **93**, 1004 (1954).

⁵ K. Suzuki, T. Kaneko, H. Yoshida, H. Morita and H. Fujimori, J. Alloys Comp. **224**, 232 (1995).

⁶ L. M. Corliss, N. Elliott and J. M. Hastings, Phys. Rev. **117**, 929 (1960).

⁷ R. M. Ibberson and R. Cywinski, Physica B **181**, 329 (1992).

⁸ J. D. Browne, R. R. Liddell, R. Street and T. Mills, Phys. Stat. Sol. (a) **1**, 715 (1970).

⁹ M. Nasr-Eddine, S. Sayetat and E. F. Bertaut, C. R. Acad. Sci. Paris **2691**, 574 (1969).

¹⁰ H. Nakagawa, S. Nasu, M. Takahashi and F. Kanamaru, Hyperfine Interact. **69**, 445 (1991); T. Hinomura and S. Nasu, Physica B **237-238**, 557 (1997); K. Suzuki, H. Morita, T. Kaneko, H. Yoshida and H. Fujimori, J. Alloys Comp. **201**, 11 (1993).

¹¹ Y. Tsuchiya, K. Kosuge, S. Yamaguchi, and N. Nakayama, Mat. Trans., JIM, **37**, 121 (1996); **38**, 91 (1997).

¹² D. A. Papaconstantopoulos, W. E. Pickett, B. M. Klein and L. L. Boyer, Phys. Rev. B **31**, 752 (1985).

¹³ A. Neckel, P. Rastl, R. Eibler, P. Weinberg and K. Schwarz, J. Phys. C **9**, 579 (1976).

¹⁴ V. P. Zhukov, V. A. Gubanov, O. Jepsen, N. E. Christensen and O. K. Andersen, J. Phys. Chem. Solids **49**, 841 (1998).

¹⁵ J. Häglung and G. Grimvall, Phys. Rev. B **43**, 14400 (1991).

¹⁶ H. Shimizu, M. Shirai and N. Suzuki, J. Phys. Soc. Jpn. **66**, 3147 (1997); **67**, 922 (1998).

¹⁷ A. Mavromaras, S. Matar, B. Siberchicot and G. Demazeau, J. Magn. Magn. Mater. **134**, 34 (1994).

¹⁸ L. M. Corliss, N. Elliott, and J. Hastings, Phys. Rev. **104**, 924 (1956); W. L. Roth, Phys. Rev. **110**, 1333 (1958).

¹⁹ D. A. Papaconstantopoulos, W. E. Pickett, B. M. Klein and L. L. Boyer, Nature **308**, 494 (1984); W. E. Pickett, B. M. Klein and D. A. Papaconstantopoulos, Physica B **108**, 667 (1981).

²⁰ J. Chen, L. L. Boyer, H. Krakauer, and M. J. Mehl, Phys. Rev. B **37**, 3295 (1988).

²¹ D. M. Ceperley and B. J. Alder, Phys. Rev. Lett. **45**, 566 (1980). J. P. Perdew and A. Zunger, Phys. Rev. B **23**, 5048 (1981).

²² D. Vanderbilt, Phys. Rev. B **32**, 8412 (1985); K. Laasonen, A. Pasquarello, R. Car, Changyol Lee, and D. Vanderbilt, Phys. Rev. B **47**, 10142 (1993).

²³ E. G. Moroni, G. Kresse, J. Hafner and J. Furthmüller, Phys. Rev. B **56**, 15629 (1997).

²⁴ S. G. Louie, S. Froyen, and M. L. Cohen, Phys. Rev. B **26**, 1738 (1982).

²⁵ H. Sawada, Y. Morikawa, K. Terakura and N. Hamada, Phys. Rev. B **56**, 12154 (1997).

²⁶ D. J. Singh and B. M. Klein, Phys. Rev. B **46**, 14969 (1992).

²⁷ W.E. Pickett, P.B. Allen, and H. Krakauer, Phys. Rev. B **38**, 2721 (1988).

²⁸ N. Chetty and R. M. Martin, Phys. Rev. B **44**, 5568 (1991); **54**, 6074 (1992).

²⁹ A. Filippetti and V. Fiorentini (to be published).

TABLE I. E_c^{th} denotes energies (in eV/formula unit) for cubic structures calculated at the theoretical a_0 of the respective phases; E_c^{ex} 's are relative to the experimental a_0 for all phases. E_d^{th} 's and E_d^{ex} 's are the same as before but now the structures are distorted by the observed change of angle α . All energies are referred to the that of the most stable structure, i.e. the AFM $_{[110]}^2$ phase with theoretical a_0 and distorted α . m 's are magnetic moments (in μ_B /metal atom).

	AFM $_{[110]}^2$	AFM $_{[110]}^1$	AFM $_{[111]}$	FM	PM
E_c^{ex}	0.068	0.034	0.085	0.110	0.273
E_c^{th}	0.068	0.033			0.259
E_d^{ex}	0.020	0.043		0.085	0.244
E_d^{th}	0				0.235
m^c	2.17	1.90	2.28	1.92	
m^d	2.15	1.94		2.08	

TABLE II. Band-by-band, and total, values of the band filling (in electrons per Cr $_4$ N $_4$ cell), DOS at the Fermi level (states/eV), and the rms values of the Cartesian components of the Fermi velocity (10^8 cm/s). The last line gives the total electrons and DOS, and the rms velocities at E_F for all four bands.

Band	Occupation	N(E_F)	v_x	v_y	v_z
1	1.97	0.73	0.084	0.056	0.061
2	1.93	1.67	0.10	0.063	0.036
3	0.10	0.93	0.16	0.16	0.25
4	0.002	0.08	0.12	0.16	0.074
Total	4.00	3.41	0.12	0.10	0.14

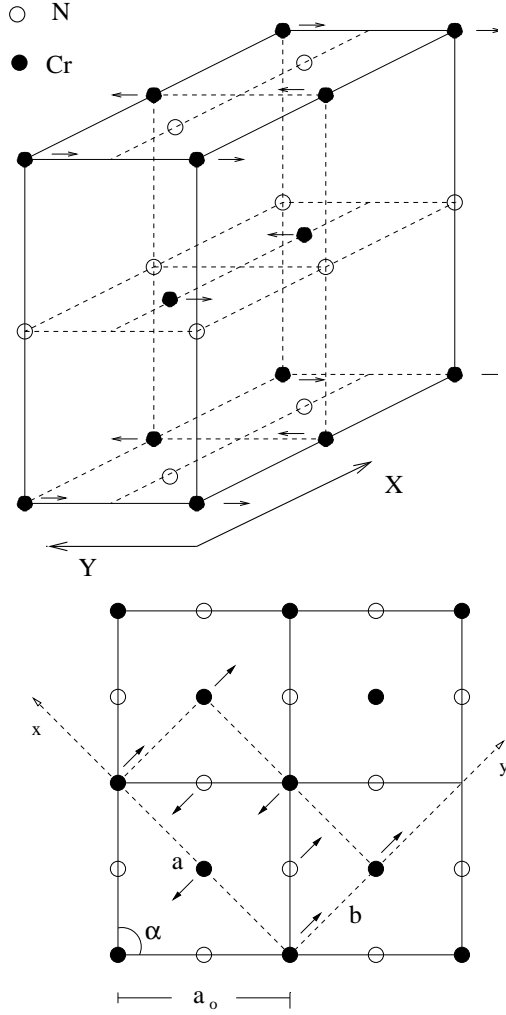


FIG. 1. Top panel: perspective view of the CrN orthorhombic cell with antiferromagnetic spin arrangement consisting of alternating double ferromagnetic layers parallel to the $[110]$ (following Corliss *et al.*). Arrows denote the relative spin directions on Cr atoms in the Néel state. Bottom panel: Top view of (001) plane. The dashed line indicates the orthorhombic cell with respect to the cubic structure.

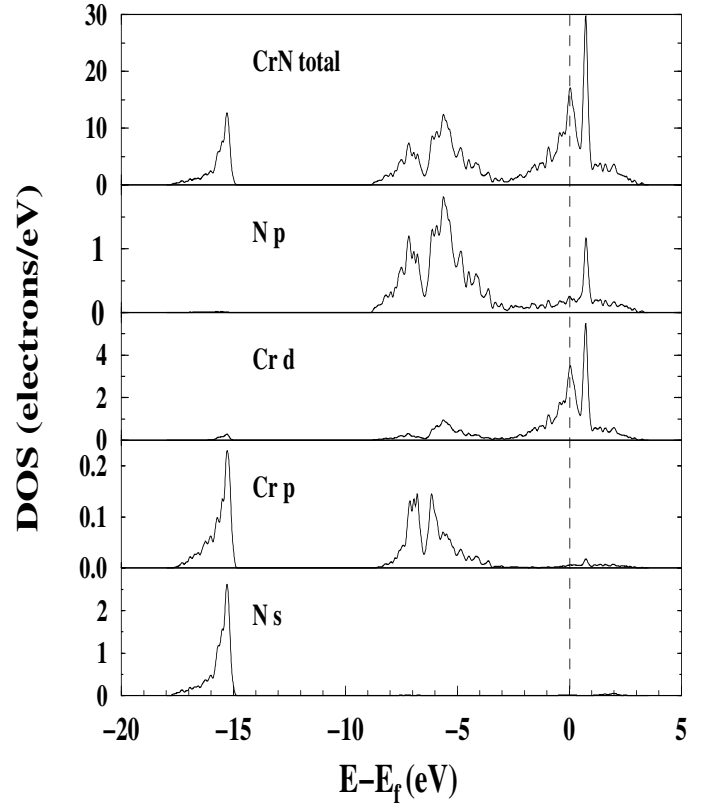


FIG. 2. Density of states of cubic PM CrN. Top panel show the total DOS, the panels below show the major contributions resolved by angular momentum character. The sharp peak at E_F is entirely Cr d (note that the N p contribution is smooth through this region).

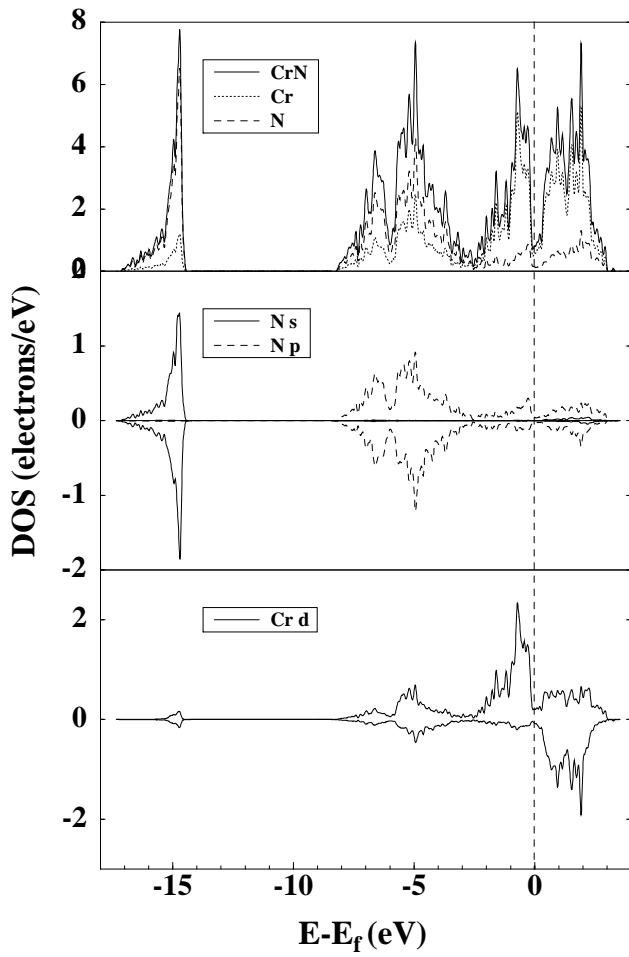


FIG. 3. Density of states of cubic AFM CrN. Top panels show total and atom by atom DOS, middle and bottom panels some contributions resolved by angular-moment.

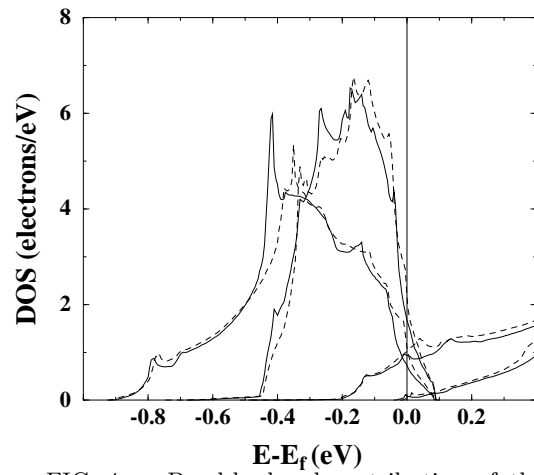


FIG. 4. Band-by-band contribution of the four bands around the Fermi level, for both cubic (dashed line) and distorted (full line) $\text{AFM}_{[110]}^2$ structure.

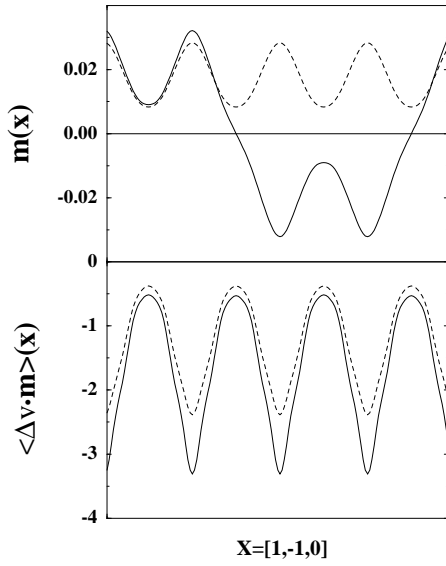


FIG. 5. Top panel: the planar average of local magnetization (in units μ_B/bohr) is pictured along the $\hat{x} = [1\bar{1}0]$ direction of the orthorhombic cell for FM (dashed line) and $\text{AFM}_{[110]}^2$ (full line) phases. Bottom panel: planar averages (in $\text{Ryd} \cdot \mu_B/\text{bohr}$) of the corresponding exchange-correlation potential splittings (see text).

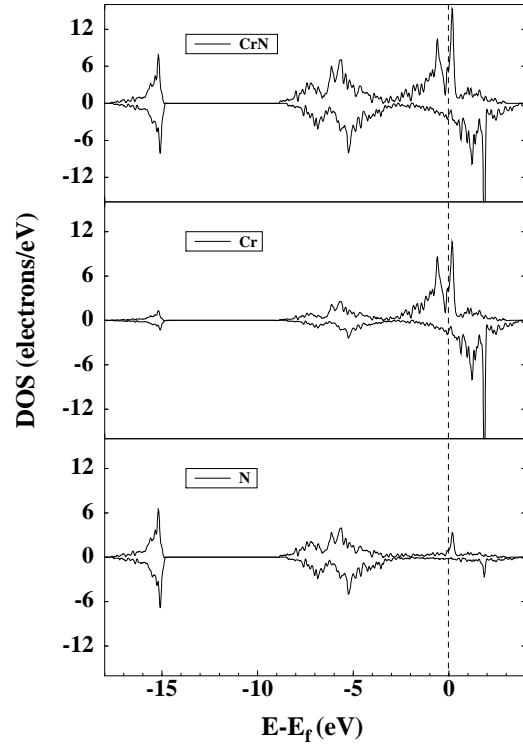


FIG. 6. Density of states of FM CrN calculated in the experimental structure. Top panel is the total DOS, lower panels show the individual contributions of each atom, as indicated in the Figure.

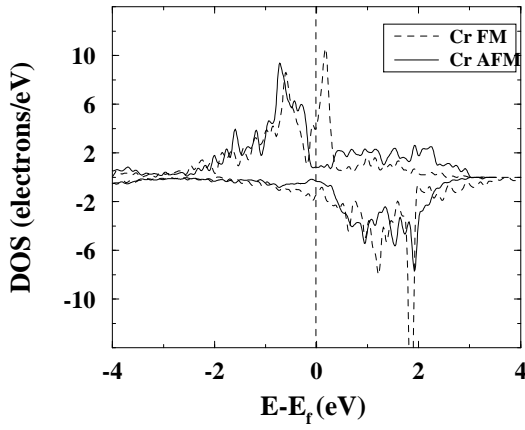


FIG. 7. Contributions of Cr to total DOS: comparison between AFM $^2_{[110]}$ and FM results.

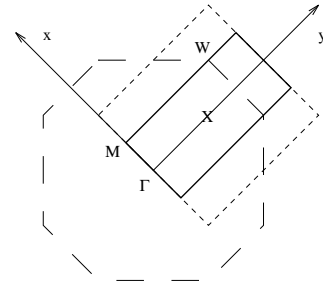
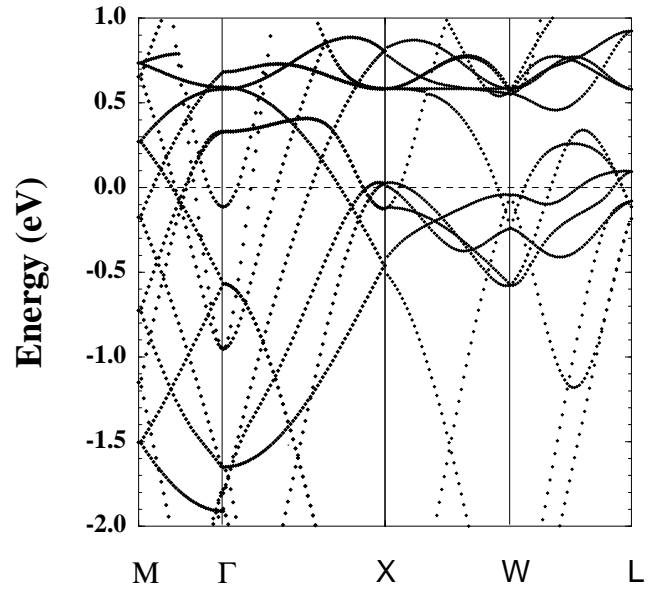


FIG. 8. Top: band structure for cubic PM CrN in the orthorhombic BZ. Energies between points M and X are for the cubic structure, where between X and L are for the distorted one, so that at X the minor band splitting due to the distortion is visible. Bottom: high symmetry points of the CrN BZ. Full line denotes the orthorhombic BZ, dashed line the cubic BZ and long-dashed line the fcc truncated octahedron.

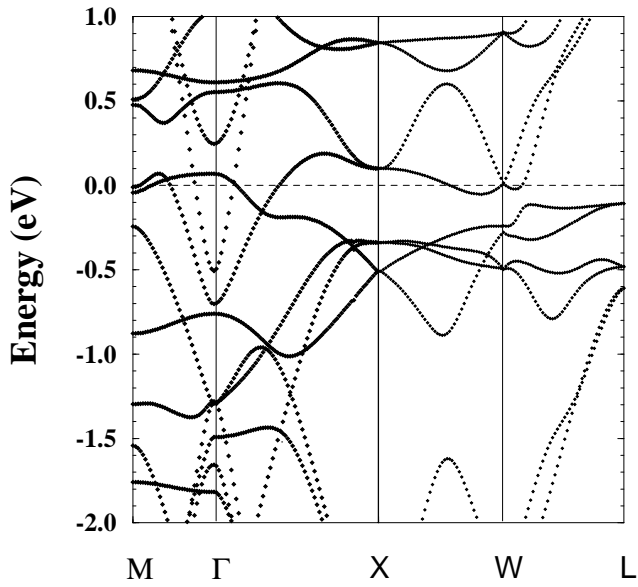


FIG. 9. Band structure for the cubic $\text{AFM}_{[110]}^2$ CrN. At variance with the PM structure, the double degeneracy at points M and W due to the cubic-to-orthorhombic downfolding is broken by the $\text{AFM}_{[110]}^2$ symmetry, thus allowing the (mostly Cr d-like) bands to be shifted out from the E_F .

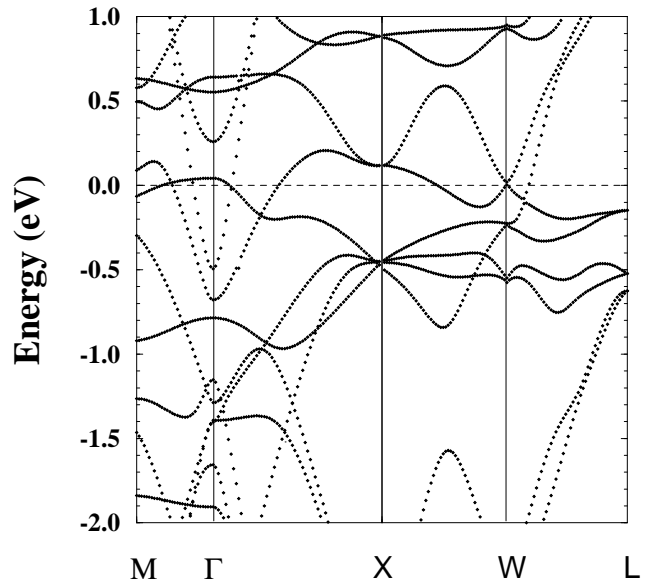


FIG. 10. Band structure for the distorted $\text{AFM}_{[110]}^2$ CrN. Lifting of degeneracies can be observed, but there are no dramatic changes with respect to the cubic $\text{AFM}_{[110]}^2$ structure.